Since January 2020 Elsevier has created a COVID-19 resource centre with free information in English and Mandarin on the novel coronavirus COVID-19. The COVID-19 resource centre is hosted on Elsevier Connect, the company's public news and information website.

33

Artificial intelligence–based solutions for early identification and classification of COVID-19 and acute respiratory distress syndrome

Sujathakrishamoorthy[1], Surapaneni Krishna Mohan[2], Veeraraghavan Vishnu Priya[3], R. Gayathri[4], M. Lorate Shiny[5]

[1]*DEPARTMENT OF COMPUTER SCIENCE, WENZHOU KEAN UNIVERSITY, ZHEJIANG PROVINCE, WENZHOU, CHINA;* [2]*DEPARTMENT OF BIOCHEMISTRY, PANIMALAR MEDICAL COLLEGE HOSPITAL AND RESEARCH INSTITUTE, CHENNAI, TAMIL NADU, INDIA;* [3]*DEPARTMENT OF BIOCHEMISTRY, SAVEETHA DENTAL COLLEGE, SAVEETHA INSTITUTE OF MEDICAL AND TECHNICAL SCIENCES, CHENNAI, TAMIL NADU, INDIA;* [4]*DEPARTMENT OF BIOCHEMISTRY, SAVEETHA DENTAL COLLEGE AND HOSPITALS, SAVEETHA INSTITUTE OF MEDICAL AND TECHNICAL SCIENCES, CHENNAI, TAMIL NADU, INDIA;* [5]*COMPUTER SCIENCE AND ENGINEERING DEPARTMENT, SRI SAIRAM COLLEGE OF ENGINEERING, BANGALORE, KARNATAKA, INDIA*

1. Introduction

A massive group of viruses, called coronaviruses, includes COVID-19. They are highly dangerous pathogens for humans that initially affect the respiratory system and cause hepatic, gastrointestinal, and neurologic disease. Mostly, they spreads to human, birds, and wild animals. Outbreaks of two existing coronaviruses, severe acute respiratory syndrome (SARS)-CoV and Middle East respiratory syndrome coronavirus, confirmed contamination between animals and humans [1–4]. The World Health Organization acquired notification from China about severe cases of respiratory infection that visited the seafood market at Wuhan. Wuhan city underwent an outbreak of novel coronavirus, called COVID-19 (also known as 2019-nCoV). Wang et al. [5] showed that COVID-19 was derived from bats, identical to two bat-derived coronavirus strains. Therefore, the origination of COVID-19 has not been confirmed and needs a closer examination.

Severe cases were identified in Wuhan city; hence, on Jan. 23, 2020, Wuhan was under lockdown, in which people were not allowed to move outside and administrators blocked all types of transport, including airports, trains, metros, and common buses to

Data Science for COVID-19. https://doi.org/10.1016/B978-0-12-824536-1.00024-1

eliminate the spread of COVID-19. Furthermore, most cities in Hubei province had a lockdown. Therefore, various kinds of cases were prevented in Chinese cities and 24 countries were affected, which were comparatively lower than Wuhan city [6–9]. The Centers for Disease Control and Prevention (CDC) confirmed the transmission of COVID-19 to humans.

Based on the CDC, COVID-19 is an airborne disease transmitted by close contact and touching surfaces and things with viral particles, and partially from fecal transmission [10–12]. The severe problem of COVID-19 is the isolation time, which is around 14 days, as defined in Nguyen [13]; over those days, the virus might be spread. In addition, in Jin et al. [14] and Wynants et al. [15] research reference based on Chinese community states that the minimum isolation time would be 3 days that is for 24 days. Hence, cases of the virus increases day by day especially in China. The spread of the virus seems to be highly dangerous and needs strong protection to save the life and policies to make sure people are unallowed to step out of house that has been executed in major cities in China, specifically in Hubei province [16–19].

Zhao et al. [20] presented arithmetic methods to compute the actual value of COVID-19 cases in Jan. 2020. The number of unpredicted cases was about 469 cases from Jan. 1 to 15, 2020. Also, after Jan. 17, 2020, the disease improved to 21-fold. Nishiura et al. [21] employed a calculation technique to measure COVID-19 in Wuhan, China applies the derived details of people who have displaced from Wuhan from Jan. 29 to 31, 2020.

Finally, it was concluded that the calculated value was higher and death rate was 0.3–0.6%. Tang et al. [22] used a numeric approach to determine the risk of spread for COVID-19 and the computed value of confirmed cases in 7 days. The highest range may be attained in 2 weeks. In Thompson [23], details of 47 patients were sampled to evaluate the transmission of COVID-19 in a human-to-human module. The researchers revealed that transmission was 0.4 and hospitalization was partial from tested data; transmission may be around 0.012 [24] and also projected a computing technique to measure the death rate due to COVID-19. The attained results for two diverse cases are 5.1% and 8.4%, respectively. In addition, the reproduction value for these two scenarios, the computed outcome depicts that COVID-19 leads to a pandemic. Massive work has been projected to detect the epidemic; for instance, DeFelice et al. [25] used a compartment approach to predict spillover communication risk as well as human West Nile virus (WNV) cases. Those technologies were applied to past information of WNY outbreaks on Long Island, New York.

Ture and Kurt [26] compared various time sequence detecting methods to detect hepatitis A virus infection. The researchers applied previous years of detail in Turkey to sample four time series detection approaches. The results of the comparative task showed that multilayer perceptron performs better than other techniques. Shaman and Karspeck [27] used a detection approach according to the ensemble adjustment Kalman filter for periodic outbreaks of virus. It computes the projected approach with the help of data on influenza seasons in New York City for 6 years (2003–08).

Also, Shaman et al. [28] defined a regular prediction for viruses using susceptible-infected-recovered-susceptible, Kalman filter, and influenza-like illness. Massad et al. [29]

used an arithmetic approach to investigate and detect the infection of the SARS epidemic. The reproduction values for two various groups, Hong Kong and Toronto, were 1.2 and 1.32, respectively. This chapter presents an enhanced kernel support vector machine (E-KSVM) to detect COVID-19 and acute respiratory distress syndrome (ARDS). The E-KSVM model operates on three levels: preprocessing, feature extraction, and classification. Once the images are preprocessed, Hough transform (HT) is applied as a feature extractor and the E-KSVM model is employed as a classifier. The KSVM is enhanced by the use of the particle swarm optimization (PSO) algorithm to tune the parameters of KSVM. An extensive set of experimentation takes place on a chest X-ray dataset and the classification of images takes place for three categories: normal, COVID-19, and ARDS.

2. The proposed enhanced kernel support vector machine model

Fig. 33.1 shows the working process of the E-KSVM model. The input image undergoes preprocessing in which unwanted details and noise that exist are discarded. Then, features in the preprocessed image are extracted by the HT. Then, the E-KSVM model is executed to classify the feature vectors into appropriate classes: normal, COVID-19, and ARDS.

2.1 Preprocessing

The images gathered from a database might have irregular data as well as background noise. Here, the preprocessing phase is mostly applied to eliminate noise from computed tomography (CT) images and develop noise-free images applicable for future computations. Various morphological tasks have been processed to produce a mask. Dilation and hole filling are core tasks in some references from a binary edge map of an image under the application of a gradient driven threshold approach:

$$f(x,y) = \begin{cases} 1 & if \;\; G(x,y) \geq GT \\ 0 & else \end{cases} \tag{33.1}$$

where GT is the gradient threshold that applies Otsu's adaptive framework. The binary image is dilated with the help of a diamond structuring component. Then, the mask is improved with an actual image. The two predefined images depict the mask produced by a gradient model and a label removed image. The key objective of a dilation task in the binary image is to introduce a higher lung region to compute in the further stage. The major step in future is to avoid the pectoral image from CT images. Such muscles are composed with nearer intensity measures compared with tumor intensity. Thus, the muscle had to be rejected from an image to attain the effective feature extraction with the application of a maximization approach, also termed segmentation models. As a result, it classifies data values

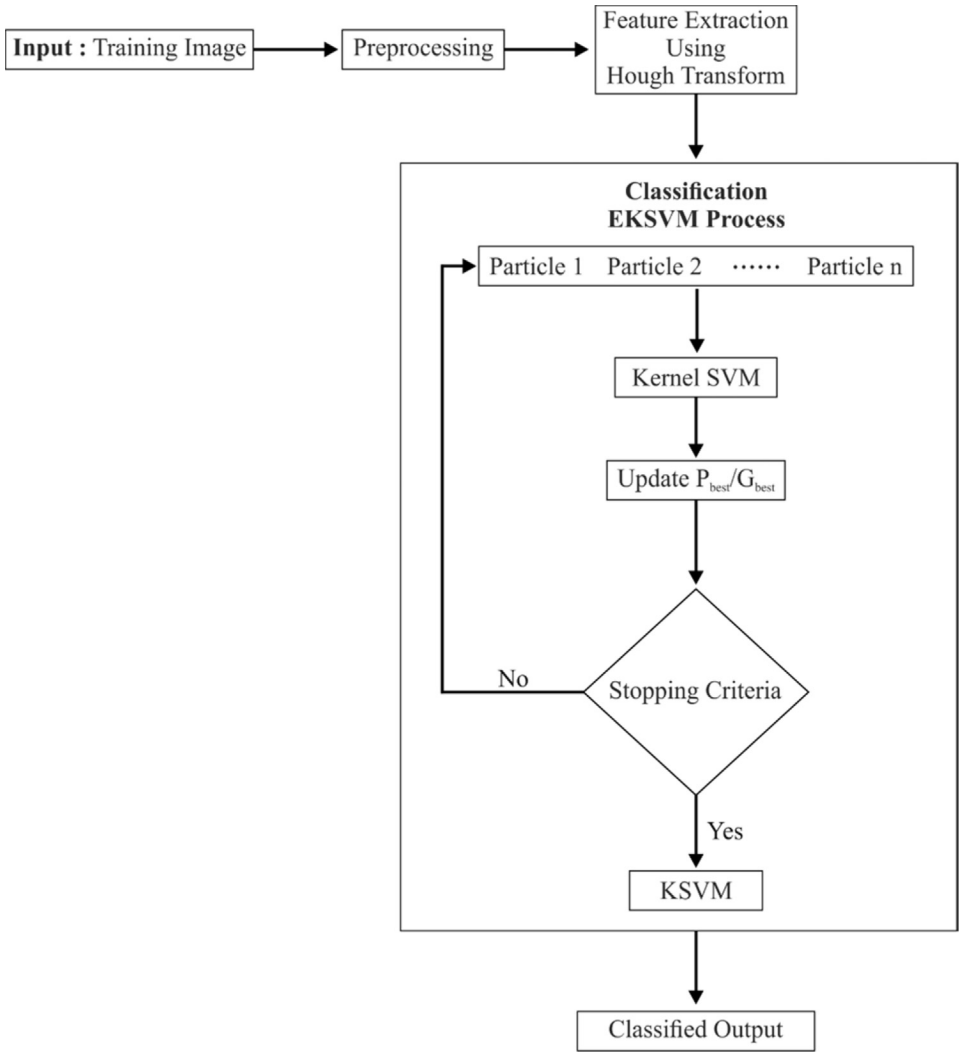

FIGURE 33.1 Workflow of enhanced kernel support vector machine (E-KSVM) model.

according to the higher likelihood condition. The major constraint for maximization determination is:

$$L\theta = Ln(P(X\theta)) \tag{33.2}$$

The application of equation maximization provides a feasible way to compute the maximum likelihood function. To eliminate the pectoral muscle and maintain the remaining lung region, four intensity class segmentations were processed on CT images under the application of maximum estimation.

2.2 Feature extraction using Hough transform

Hough transform is defined as the feature extraction method applied in digital signal processing to evaluate shape parameters from corresponding boundary points. Hence, HT has been used to detect random shapes. Normal parameterization is provided by:

$$x \cos \theta + y \sin \theta = \rho \tag{33.3}$$

HT is referred as a tolerant space in edges and is free from noise, which is a derivation of arbitrary transform. It provides points from a diverse angle. Canny edge prediction is applied in the preprocessed image before employing the HT. In addition, it projects an optimal edge prediction filter to split the edges with the application of the first derivative of a Gaussian. These operations are used to decrease the preprocessing duration and offer a reliable data source that withstands geometrical as well as ecological modifications to calculate HT. It applies measures for every edge point (X, Y) for the image estimated from the given function. In addition, nonanalytical space is estimated in Eq. (33.5) with a particular batch of boundary points. For shape q, it is named P in Eq. (33.6):

$$\rho = X_i \cos \theta + Y_i \sin \theta \tag{33.4}$$

$$B = \{X_B\} \tag{33.5}$$

$$p = \{X^o, s, \theta\} \tag{33.6}$$

For each X_B, r is calculated and it stored as function φ. The value for r for each pixel X of gradient function $\varphi(X)$ in an image is calculated in Eq. (33.8) and is stored in the accumulator:

$$r = X^o - X_B \tag{33.7}$$

$$A(X + r) \tag{33.8}$$

Under the application of an accumulator, HT results in preprocessed CT images. Then, some features are selected from the transform image. Only the effective features should be selected; inefficient features might decrease the efficiency of the classification model. Here, the work intensity features were chosen and the application of these features results from the complexity of interpretation. It has the well-defined masses, speculated mass, ill-defined mass, architectural distortion, asymmetry, and so on. The intensity features applied for mean, variance, entropy, and standard deviation are highly effective.

2.3 Particle swarm optimization–kernel support vector machine classifier

2.3.1 Support vector machine classifier

Many enhanced methods in SVM are deployed and the KSVM is a well-known and productive technique. Therefore, the merits of KSVM are that it can be processed from diverse scenarios for natural language processing, biomedical, and computer visibility; there are few tunable parameters; and training often employs quadratic optimization.

Thus, the main aim is to remove the combined local minimum depicted by alternate statistical learning models such as neural networks.

2.3.1.1 Principles of linear support vector machines

Let the p-dimensional training dataset of size N be:

$$\{(x_n, y_n)|x_n \in R^p, y_n \in \{-1, +1\}\}, \quad n = 1, \ldots, N \tag{33.9}$$

where y_n is either -1 *or* 1 implies the class 1 *or* 2. Each x_n is a p-dimensional vector. The maximum-margin hyperplane that divides class 1 from class 2 is task of SVM. In general, the hyperplane is described as provided in Eq. (33.10):

$$WX - b = 0 \tag{33.10}$$

where $\cdot$ shows the dot product and w is a normal vector. There is a requirement to choose *wandb* to improve the margin from two parallel hyperplanes. Hence, two hyperplanes can be represented as:

$$WX - b = \pm 1 \tag{33.11}$$

This task has been assumed to be an optimization issue. It is the main aim is to enhance the distance from two parallel hyperplanes, which refers to removing data falling into a margin. With the application of easy numerical knowledge, the issue can be expressed as:

$$\min_{w,b} \|w\| \tag{33.12}$$

$$s.t. y_n(wx_n - b) \geq 1, \quad n = 1, \ldots, N$$

Specifically, $\|w\|$ has been replaced with:

$$\min_{w,b} \frac{1}{2}\|w\|^2 \tag{33.13}$$

$$s.t. y_n(wx_n - b) \geq 1, \quad n = 1, \ldots N$$

2.3.1.2 Soft margin

Practically, there is a lack of hyperplanes that divides the methods effectively. To solve the issue, a soft margin approach was used that selects a hyperplane to divide accessible instances with the limitation of an increasing distance of closer samples. A positive slack variable ξ_n is established to choose the degree of misclassifying sample x_n. Then, the optimal hyperplane that isolates the data might be attained by using Eq. (33.14):

$$\min_{W,\xi,b} \frac{1}{2}\|w\|^2 + P\sum_{n=1}^{N} \xi_n \tag{33.14}$$

$$s.t. \begin{cases} y_n(wx_n - b) \geq 1 - \xi_n \\ \xi_n \geq 0, \end{cases} n = 1, \ldots, N$$

where P represents the error penalty. Therefore, the optimization is developed as a trade-off for a big margin as well as tiny error penalty. The restraint optimization problem can be resolved under the application of a Lagrange multiplier:

$$\min_{w,\xi,b}\ \max_{\alpha,\beta}\left\{\frac{1}{2}\|w\|^2+P\sum_{n=1}^{N}\xi_n-\sum_{n=1}^{N}\alpha_n[y_n(wx_n-b)-1+\xi_n]-\sum_{n=1}^{N}\beta_n\xi_n\right\} \tag{33.15}$$

The min-max problem is hard to predict; thus, the dual form model is applied to deal with such a problem.

2.3.1.3 Dual form

Eq. (33.14) might be equated as:

$$\max_{\alpha}\ \sum_{n=1}^{N}\alpha_n-\frac{1}{2}\sum_{n=1}^{N}\sum_{m=1}^{N}\alpha_m\alpha_n y_m y_n K(x_m,x_n) \tag{33.16}$$

$$s.t\begin{cases}0\le\alpha\le C,\\ \sum_{n=1}^{N}\alpha_n y_n=0,\end{cases}\quad n=1,\dots,N$$

A benefit of the dual form is the absence of slack variables, ξ_n, along with constant C, which exists from the shortcomings of Lagrange multipliers.

2.3.2 Kernel support vector machine

Linear SVM is composed with limitations on the linear hyperplane, which is capable of dividing complex realistic data. To normalize in the form of nonlinear hyperplane, the main objective is applied to SVM. The final method is scientifically the same; each dot product is replaced with a nonlinear kernel function. The KSVM allocated the maximum-margin hyperplane from a converted feature space. The transmission may be nonlinear, and converted space may be highly dimensional. Although the classifier is a hyperplane from a high-dimensional feature space, it can be nonlinear in an imaginative input space. For a single kernel, the least variable is required to develop a kernel as flexible and to modify it for practical data. It is applied with an radial basis function (RBF) kernel because it is efficient for producing a remarkable outcome. The kernel is expressed as:

$$k(x_a,x_b)=\exp\left(-\frac{\|x_a-x_b\|}{2\sigma^2}\right) \tag{33.17}$$

Now, Eq. (33.17) would be used in Eq. (33.18) to attain the consequent training function of SVM in Eq. (33.19):

$$\max_{\alpha}\sum_{b=1}^{N}\alpha_b-\frac{1}{2}\sum_{b=1}^{N}\sum_{a=1}^{N}\alpha_a\alpha_b y_a y_b k(x_a,x_b) \tag{33.18}$$

$$\max_{\alpha}\sum_{b=1}^{N}\alpha_b-\frac{1}{2}\sum_{b=1}^{N}\sum_{a=1}^{N}\alpha_a\alpha_b y_a\alpha_b\exp\left(-\frac{\|x_a-x_b\|}{2\sigma^2}\right) \tag{33.19}$$

2.3.3 Particle swarm optimization—kernel support vector machine

The PSO technique has been used to process parameter optimization. Also, it is a global optimization method accelerated from the behavior of bird flocking or fish schooling. It is a simple to model and provides rapid execution. PSO computes the searching task by using a set of particles maximized for each iteration. To derive the best solutions, all particles have to be shifted in the direction of preceding best (p_{best}) and best global (g_{best}) positions in the swarm:

$$p_{best_m} = p_m(k^*) \tag{33.20}$$

$$st.fitness(p_m(k^*)) = \min_{k=1,\dots,t} [fitness(p_m(k))],$$

$$g_{best} = p_{m^*}(k^*) \tag{33.21}$$

$$s.t.fitness(p_m(k^*)) = \min_{\substack{m=1,\dots,p \\ k=1,\dots,t}} [fitness(p_m(k))]$$

where m is a particle index, P implies the particle number, k denotes a round index, t refers to the iteration value, and p is a position [30]. The extension of velocity and position of particles are carried out by applying Eqs. (33.22) and (33.23):

$$V_m(t+1) = wv_m(t) + c_1 r_1(p_{best_m}(t) - p_m(t)) + c_2 r_2(g_{best}(t) - p_m(t)) \tag{33.22}$$

$$p_m(t+1) = p_m(t) + V_m(t+1) \tag{33.23}$$

where V is the velocity. Inertia weight w used to manage global exploration and local exploitation. r_1 and r_2 are uniformly distributed with random parameters from the range of $(0, 1)$ c_1 and c_2 are acceleration coefficients. At this point, particle encoding is operated with variables C and σ in Eq. (33.22).

2.4 Cross-validation

This work employs the computation of fivefold cross-validation to attain the best trade-off from processing complexity as well as reliability evaluation. The whole dataset is divided into five mutually unique subsets with same size, which have four subsets for training; the last subset is used to test the model. It has been iterated around five times; hence, each subset is applied in testing. The five fold (FF) of the PSO model to select the classifier accuracy is:

$$fitness = \frac{1}{5} \sum_{i=1}^{5} \left| \frac{y_s}{y_s + y_m} \right| \tag{33.24}$$

where y_s and y_m are the number of effective classification and misclassification, respectively. PSO is implemented for a higher FF function.

3. Experimental validation

The dataset holds a set of 30 images, including 10 images each for the COVID-19 [31], ARDS, and normal categories. Some sample images in the three categories are shown in Fig. 33.2.

Table 33.1 provides a comparative analysis of models. Fig. 33.3 depicts a comparative analysis with respect to sensitivity and specificity. The random tree (RT) method requires a lower sensitivity and specificity of 72.34% and 69.04% whereas the SVM approach attains a better sensitivity and specificity of 70.58% and 73.49%. However, the E-KSVM

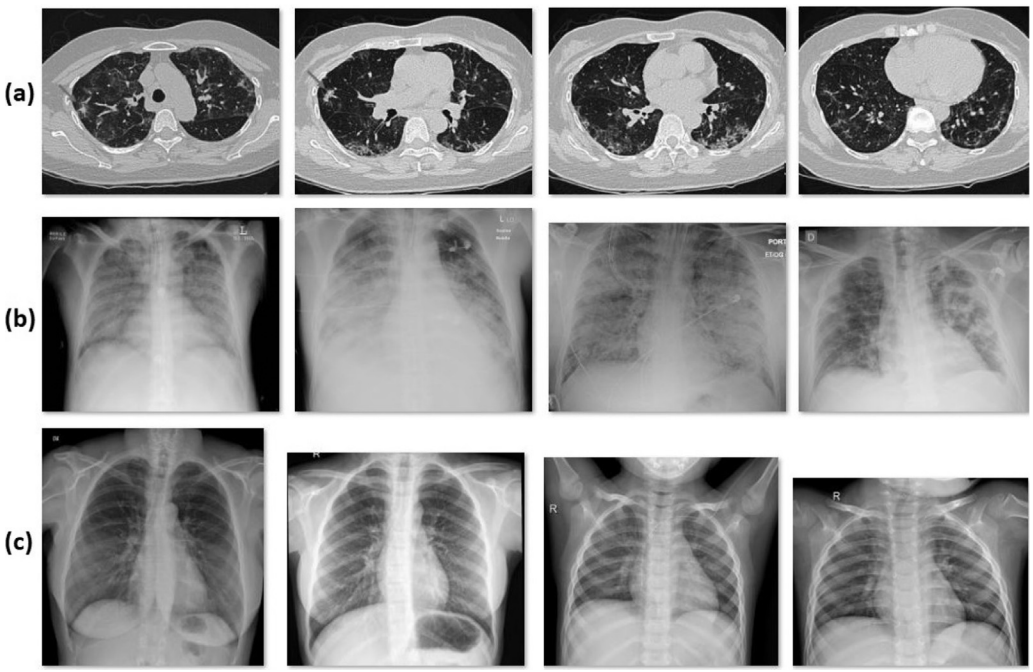

FIGURE 33.2 (A) COVID-19 images; (B) acute respiratory distress syndrome images; (C) normal images.

Table 33.1 Result of analysis of various methods.

Method	Enhanced kernel support vector machine	Support vector machine	Random tree
Sensitivity	72.34	70.58	68.30
Specificity	75.20	73.49	69.04
Accuracy	74.01	73.10	68.93
F score	73.94	72.76	66.77

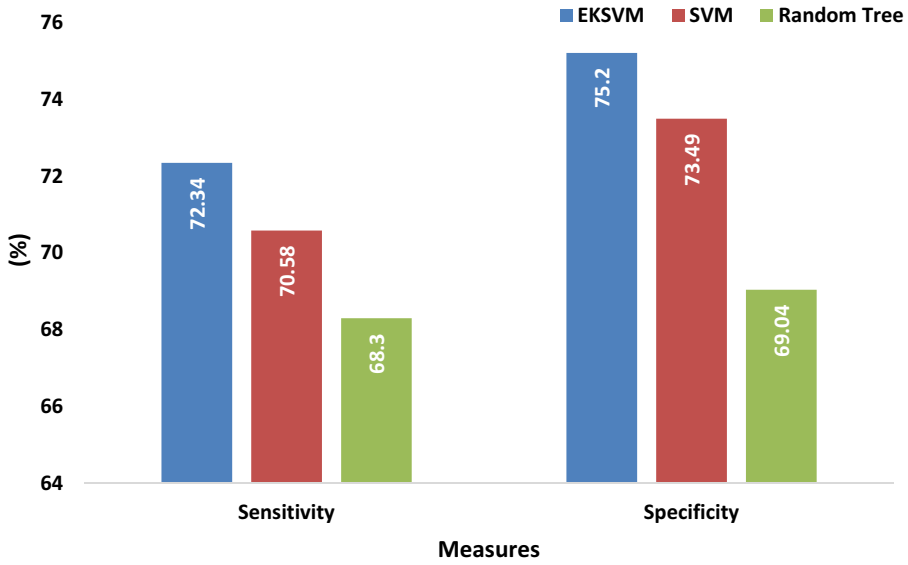

FIGURE 33.3 Comparative analysis of various methods. *EKSVM*, enhanced kernel support vector machine; *SVM*, support vector machine.

method has attained an efficient sensitivity and specificity of 72.34% and 75.20%, respectively.

Fig. 33.4 shows a comparative analysis by means of accuracy. The RT model requires an accuracy of at least 68.93% and the SVM model accomplishes a slightly moderate

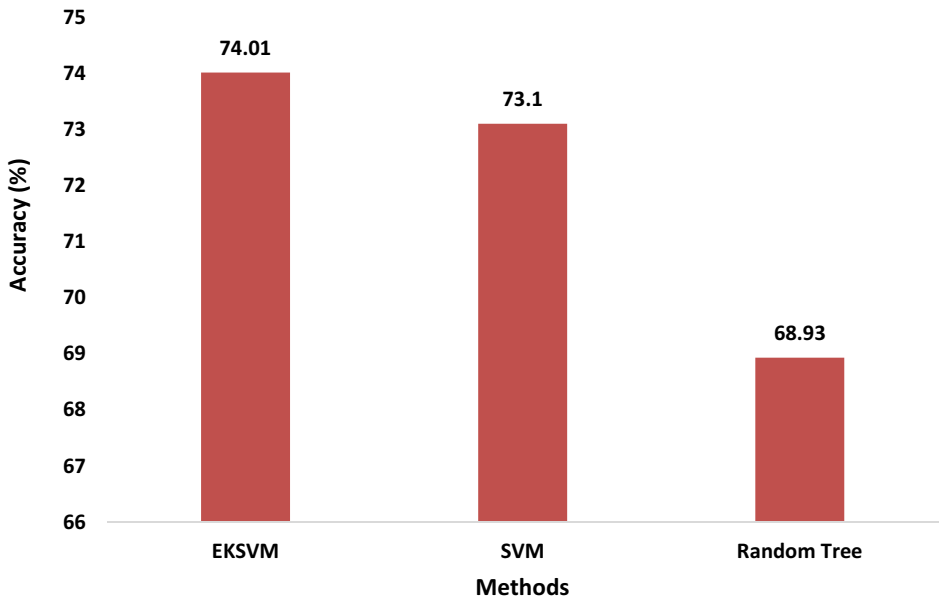

FIGURE 33.4 Accuracy analysis of existing methods. *EKSVM*, enhanced kernel support vector machine; *SVM*, support vector machine.

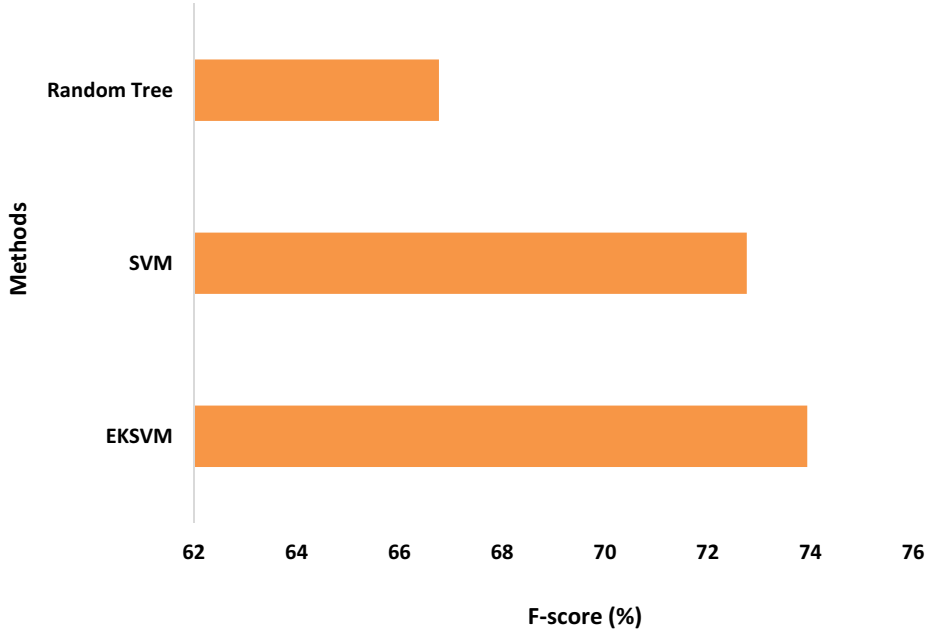

FIGURE 33.5 F score analysis of existing methods. *EKSVM*, enhanced kernel support vector machine; *SVM*, support vector machine.

accuracy of 73.10%. Therefore, the proposed E-KSVM model has effective results and obtained a higher accuracy of 74.01%.

Fig. 33.5 shows a comparative analysis with respect to the F score. The RT model requires a lower F score of 66.77% and the SVM model accomplishes a slightly gradual F score of 72.76%. Hence, the projected E-KSVM approach has a productive outcome with the best F score of 73.94%.

Table 33.2 and Fig. 33.6 show the computation time analysis of the proposed and existing models. The RT model requires a maximum computation time of 9.362s, whereas the E-KSVM and SVM models reached a minimal computation time of 8.039 and 7.310s, respectively.

From these figures and tables, it is apparent that the EK-SVM model outperformed all earlier models regarding the successful identification of COVID-19 and ARDS. Therefore, it can be effectively used as a proper diagnosis tool in actual hospitals.

Table 33.2 Computation time analysis of various methods.

Methods	Enhanced kernel support vector machine	Support vector machine	Random tree
Computation time (s)	8.039	7.310	9.362

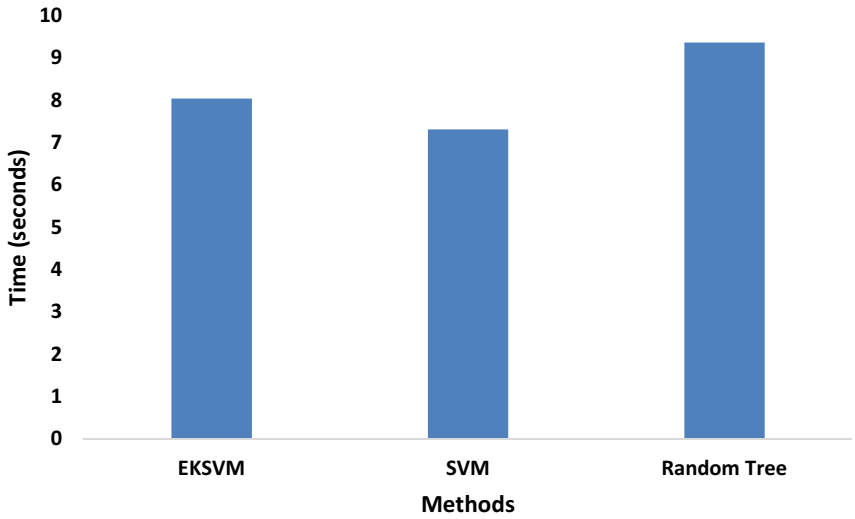

FIGURE 33.6 Computation time analysis of existing models. *EKSVM*, enhanced kernel support vector machine; *SVM*, support vector machine.

4. Conclusion

This chapter presents an E-KSVM model for the detection of COVID-19 and ARDS. The input image was preprocessed to eliminate unwanted details and noise. Then, the features in the preprocessed image were extracted by HT. Finally, the E-KSVM model was executed to classify feature vectors into appropriate classes: normal, COVID-19, and ARDS. A detailed experimental analysis was performed on a chest X-ray dataset and confirmed that the E-KSVM model has the ability to detect the disease effectively. The simulation outcome indicated that the E-KSVM model attained a maximum sensitivity of 72.34%, specificity of 75.20%, accuracy of 74.01%, and F score of 73.94% with a minimum computation time of 8.039s. In future work, the experimental outcome can be further increased using deep learning concepts.

References

[1] L. Li, L. Qin, Z. Xu, Y. Yin, X. Wang, B. Kong, J. Bai, Y. Lu, Z. Fang, Q. Song, K. Cao, Artificial intelligence distinguishes COVID-19 from community acquired pneumonia on chest CT, Radiology (March 19, 2020) 200905.

[2] F. Shi, J. Wang, J. Shi, Z. Wu, Q. Wang, Z. Tang, K. He, Y. Shi, D. Shen, Review of artificial intelligence techniques in imaging data acquisition, segmentation and diagnosis for covid-19, IEEE Rev. Biomed. Eng. 14 (2021) 4–15, https://doi.org/10.1109/RBME.2020.2987975.

[3] J. Bullock, K.H. Pham, C.S. Lam, M. Luengo-Oroz, Mapping the Landscape of Artificial Intelligence Applications against COVID-19. arXiv Preprint arXiv:2003.11336, March 25, 2020.

[4] O. Gozes, M. Frid-Adar, H. Greenspan, P.D. Browning, H. Zhang, W. Ji, A. Bernheim, E. Siegel, Rapid Ai Development Cycle for the Coronavirus (Covid-19) Pandemic: Initial Results for Automated Detection & Patient Monitoring Using Deep Learning Ct Image Analysis. arXiv Preprint arXiv:2003.05037, March 10, 2020.

[5] S. Wang, B. Kang, J. Ma, X. Zeng, M. Xiao, J. Guo, M. Cai, J. Yang, Y. Li, X. Meng, B. Xu, A deep learning algorithm using CT images to screen for Corona Virus Disease (COVID-19), MedRxiv (January 1, 2020), https://doi.org/10.1101/2020.02.14.20023028.

[6] X. Jiang, M. Coffee, A. Bari, J. Wang, X. Jiang, J. Shi, J. Dai, J. Cai, T. Zhang, Z. Wu, G. He, Towards an artificial intelligence framework for data-driven prediction of coronavirus clinical severity, Comput. Mater. Continua (CMC) 63 (1) (May 11, 2020) 537–551.

[7] A. Alimadadi, S. Aryal, I. Manandhar, P.B. Munroe, B. Joe, X. Cheng, Artificial Intelligence and Machine Learning to Fight COVID-19.

[8] R. Vaishya, M. Javaid, I.H. Khan, A. Haleem, Artificial Intelligence (AI) applications for COVID-19 pandemic, Diabetes Metab. Syndr. Clin. Res. Rev. 14 (4) (2020) 337–339.

[9] H.S. Maghdid, K.Z. Ghafoor, A.S. Sadiq, K. Curran, K. Rabie, A Novel Ai-Enabled Framework to Diagnose Coronavirus Covid 19 Using Smartphone Embedded Sensors: Design Study. arXiv Preprint arXiv:2003.07434, March 16, 2020.

[10] [10a] C. Jin, W. Chen, Y. Cao, Z. Xu, X. Zhang, L. Deng, C. Zheng, J. Zhou, H. Shi, J. Feng, Development and Evaluation of an AI System for COVID-19 Diagnosis. medRxiv, 2020 Jan 1;
[10b] B. Ghoshal, A. Tucker, Estimating Uncertainty and Interpretability in Deep Learning for Coronavirus (COVID-19) Detection. arXiv Preprint arXiv:2003.10769, March 22, 2020.

[11] H.X. Bai, B. Hsieh, Z. Xiong, K. Halsey, J.W. Choi, T.M. Tran, I. Pan, L.B. Shi, D.C. Wang, J. Mei, X.L. Jiang, Performance of radiologists in differentiating COVID-19 from viral pneumonia on chest CT, Radiology (March 10, 2020) 200823.

[12] I. Castiglioni, D. Ippolito, M. Interlenghi, C.B. Monti, C. Salvatore, S. Schiaffino, A. Polidori, D. Gandola, C. Messa, F. Sardanelli, Artificial intelligence applied on chest X-ray can aid in the diagnosis of COVID-19 infection: a first experience from Lombardy, Italy, medRxiv (January 1, 2020).

[13] T.T. Nguyen, Artificial intelligence in the battle against coronavirus (COVID-19): a survey and future research directions, Preprint 10 (2020) arXiv:2008.07343 [cs.CY].

[14] S. Jin, B. Wang, H. Xu, C. Luo, L. Wei, W. Zhao, X. Hou, W. Ma, Z. Xu, Z. Zheng, W. Sun, AI-assisted CT imaging analysis for COVID-19 screening: building and deploying a medical AI system in four weeks, medRxiv 98 (2020) 106897.

[15] L. Wynants, B. Van Calster, M.M. Bonten, G.S. Collins, T.P. Debray, M. De Vos, M.C. Haller, G. Heinze, K.G. Moons, R.D. Riley, E. Schuit, Prediction models for diagnosis and prognosis of covid-19 infection: systematic review and critical appraisal, BMJ (April 7, 2020) 369.

[16] S. Cauchemez, M. Van Kerkhove, S. Riley, C. Donnelly, C. Fraser, N. Ferguson, Transmission scenarios for Middle East Respiratory Syndrome Coronavirus (MERS-CoV) and how to tell them apart, Euro Surveill. Bull. Eur. Sur Les Mal. Transm. Eur. Commun. Dis. Bull. 18 (2013) 20503.

[17] R. Lu, X. Zhao, J. Li, P. Niu, B. Yang, H. Wu, W. Wang, H. Song, B. Huang, N. Zhu, et al., Genomic characterisation and epidemiology of 2019 novel coronavirus: implications for virus origins and receptor binding, Lancet 395 (2020) 565–574.

[18] Z.J. Cheng, J. Shan, Novel Coronavirus: Where We Are and what We Know. Infection 2020, 2019.

[19] W.J. Guan, Z.Y. Ni, Y. Hu, W.H. Liang, C.Q. Ou, J.X. He, L. Liu, H. Shan, C.L. Lei, D.S. Hui, et al., Clinical Characteristics of 2019 novel coronavirus infection in China, medRxiv (2020). Available vonline, https://www.medrxiv.org/content/early/2020/02/09/2020.02.06.20020974.full.pdf. (Accessed 9 February 2020).

[20] S. Zhao, S.S. Musa, Q. Lin, J. Ran, G. Yang, W. Wang, Y. Lou, L. Yang, D. Gao, D. He, M.H. Wang, Estimating the unreported number of novel coronavirus (2019-nCoV) cases in China in the first half of January 2020: a data-driven modelling analysis of the early outbreak, J. Clin. Med. 9 (2) (February 2020) 388.

[21] H. Nishiura, T. Kobayashi, T. Miyama, A. Suzuki, S. Jung, K. Hayashi, R. Kinoshita, Y. Yang, B. Yuan, A.R. Akhmetzhanov, N.M. Linton, Estimation of the asymptomatic ratio of novel coronavirus infections (COVID-19), medRxiv, (January 1, 2020). https://doi.org/10.1101/2020.03.17.20037432.

[22] B. Tang, X. Wang, Q. Li, N.L. Bragazzi, S. Tang, Y. Xiao, J. Wu, Estimation of the transmission risk of the 2019-nCoV and its implication for public health interventions, J. Clin. Med. 9 (2) (February 2020) 462.

[23] R.N. Thompson, Novel coronavirus outbreak in Wuhan, China, 2020: intense surveillance is vital for preventing sustained transmission in new locations, J. Clin. Med. 9 (2) (February 2020) 498.

[24] S.M. Jung, A.R. Akhmetzhanov, K. Hayashi, N.M. Linton, Y. Yang, B. Yuan, T. Kobayashi, R. Kinoshita, H. Nishiura, Real-time estimation of the risk of death from novel coronavirus (COVID-19) infection: inference using exported cases, J. Clin. Med. 9 (2) (February 2020) 523.

[25] N.B. DeFelice, E. Little, S.R. Campbell, J. Shaman, Ensemble forecast of human West Nile virus cases and mosquito infection rates, Nat. Commun. 8 (1) (February 24, 2017) 1–6.

[26] M. Ture, I. Kurt, Comparison of four different time series methods to forecast hepatitis A virus infection, Expert Syst. Appl. 31 (1) (July 1, 2006) 41–46.

[27] J. Shaman, A. Karspeck, Forecasting seasonal outbreaks of influenza, Proc. Natl. Acad. Sci. U S A 109 (50) (December 11, 2012) 20425–20430.

[28] J. Shaman, A. Karspeck, W. Yang, J. Tamerius, M. Lipsitch, Real-time influenza forecasts during the 2012–2013 season, Nat. Commun. 4 (1) (December 3, 2013), 1–0.

[29] E. Massad, M.N. Burattini, L.F. Lopez, F.A. Coutinho, Forecasting versus projection models in epidemiology: the case of the SARS epidemics, Med. Hypotheses 65 (1) (January 1, 2005) 17–22.

[30] Y. Zhang, S. Wang, G. Ji, Z. Dong, An MR brain images classifier system via particle swarm optimization and kernel support vector machine, Sci. World J. 2013 (2013).

[31] https://github.com/ieee8023/covid-chestxray-dataset.